Carbon 175 (2021) 155–163

Contents lists available at ScienceDirect

Carbon

journal homepage: www.elsevier.com/locate/carbon

Research Article

Growth of high-quality wafer-scale graphene on dielectric substrate for high-response ultraviolet photodetector

Yang Chen [a, b], Ke Jiang [a, b], Hang Zang [a, b], Jianwei Ben [a, c], Shanli Zhang [a, b], Zhiming Shi [a, b], Yuping Jia [a, b], Wei Lü [a, d], Dabing Li [a, b], Xiaojuan Sun [a, b, *]

[a] State Key Laboratory of Luminescence and Applications, Changchun Institute of Optics, Fine Mechanics and Physics, Chinese Academy of Sciences, Changchun, 130033, China
[b] Center of Materials Science and Optoelectronics Engineering, University of Chinese Academy of Sciences, Beijing, 100049, China
[c] College of Materials Science and Engineering, Shenzhen University, Shenzhen, 518071, China
[d] Key Laboratory of Advanced Structural Materials, Ministry of Education, Changchun University of Technology, Changchun, 130012, China

ARTICLE INFO

Article history:
Received 29 September 2020
Received in revised form
12 December 2020
Accepted 17 December 2020
Available online 21 December 2020

Keywords:
Graphene
Graphene growth
Ni/SiO_2 capping layer
Dielectric substrate
Ultraviolet photodetector

ABSTRACT

Growth of graphene on dielectric substrates is crucial for its use in various electronic and optoelectronic devices, which may avoid the additional extrinsic defects and residual pollution originating from the essential transfer process of graphene grown by chemical vapor deposition on metal foils. However, the growth of high-quality and wafer-scale graphene on dielectric substrates is now still a challenge. Herein, we report the growth of graphene from solid polymer carbon source on various substrates under the assistance of Nickel/SiO_2 capping layer. The wafer-scale graphene with excellent uniformity and continuity was achieved on 2 inch sapphire substrates. The dynamics of the graphene growth were proposed, which mainly consist of polymer carbonization, carbon dissolution, segregation and precipitation. The graphene was also grown on undoped GaN to serve as the carrier transport channel of ultraviolet photodetectors, exhibiting a 4 A/W response. The growth of high-quality and wafer-scale graphene on dielectric substrates reported by present work would promote commercial application of the graphene-based electronic and optoelectronic devices.

© 2020 Elsevier Ltd. All rights reserved.

1. Introduction

Since graphene was firstly mechanically exfoliated from highly oriented pyrolytic graphite in 2004 [1], it has shown significant applications in advanced electronic and optoelectronic devices including transistors [2–4], light-emitting diodes [5,6], photodetectors [7–9], solar cells [10], and supercapacitors [11,12], which mainly benefits from its unique properties of high carrier mobility, perfect transparency, and feasible flexibility [13]. Moreover, the weak van der Waals interlayer force provided by graphene has triggered the extensive study of high-quality and stress-free nitrides epitaxy using graphene as the buffer layer [14–16]. To explore more efficient methods for graphene growth, various strategies such as liquid phase exfoliation [17,18], reduction of graphene oxide [19,20], pyrogenic decomposition of SiC [21,22], and chemical vapor deposition (CVD) [23–25] have been developed. Among them, the catalytic growth of graphene on metal foils (Nickel or Copper) by CVD is regarded as a promising strategy due to its inch-production, high crystallinity, and controlled layer thickness [26]. However, it involves a meticulous and complicated transfer process from catalytic metal foils to dielectric substrates, which might cause residual pollution and additional extrinsic defects as well as cracks [27,28]. To overcome this bottleneck, graphene was directly grown on glass substrates by CVD method [29,30]. However, the carbon precursor decomposition on these non-catalytic substrates exhibits higher energy barrier, and thus the rigorous growth temperature (1100 °C) and long growth time (few hours) are required. More importantly, it is difficult to obtain the graphene on non-catalytic glass substrates with the same quality as that on metal foils.

The growth of graphene on dielectric substrates can also be achieved from solid organic carbon source [31–33]. Usually, polystyrene, polymethyl methacrylate (PMMA) and polycyclic aromatic

* Corresponding author. State Key Laboratory of Luminescence and Applications, Changchun Institute of Optics, Fine Mechanics and Physics, Chinese Academy of Sciences, Changchun, 130033, China.
E-mail address: sunxj@ciomp.ac.cn (X. Sun).

https://doi.org/10.1016/j.carbon.2020.12.055
0008-6223/© 2020 Elsevier Ltd. All rights reserved.

hydrocarbons could sever as the carbon precursors, and additional catalytic metal coverages are applied for graphene conversion during the thermal annealing process. Different from the gas precursors such as methane and ethylene, solid carbon sources could be directly deposited on arbitrary substrates by spin coating or thermal vacuum evaporation. This graphene growth method has also exhibited advantages of speediness in time and favorable growth condition. Although graphene converted from solid carbon sources is a prospective strategy to achieve the growth of graphene on dielectric substrates, several obstacles have hindered its practical application. Previous works have indicated that thin metal films (Gold, Copper and Nickel) are unstable and tend to deform into particles during the annealing process at high temperature [34–36]. As a consequence, the surface morphology of as-grown graphene would exhibit unsatisfied uniformity and continuity because of the insufficient protection of the underneath solid carbon sources associated with the catalytic metal deformation [37,38]. More importantly, the defects density of graphene converted from solid carbon materials is still higher than that grown by CVD, and the wafer-scale graphene growth for mass production demand by this strategy is facing great challenges due to the poor uniformity and continuity of as-grown graphene. In the end, the intrinsic dynamics of the growth process of this graphene need to be investigated and proposed, which might provide specific guidance for the growth of high-quality graphene.

In present work, we reported the growth of high-quality and wafer-scale graphene from polymer carbon source (PMMA) on various dielectric substrates with the Nickel/SiO_2 capping layer. The additional SiO_2 capping layer has changed the surface energy of catalytic Nickel film and enlarged its deformation energy barrier, ensuring the integrity of the Nickel/SiO_2 capping layer during the thermal annealing process. Therefore, the *in situ* growth of high-quality and wafer-scale graphene on dielectric substrates exhibited excellent uniformity and continuity. The dynamics of the growth process of this graphene were proposed, including carbonization of solid PMMA, carbon dissolution, segregation, and precipitation. The response of the ultraviolet (UV) photodetector based on graphene grown on undoped GaN (u-GaN) reached up to 4 A/W due to the high carrier mobility and persistent photoconduction effect of the top graphene, which well demonstrated the feasibility and practicability of this graphene growth strategy.

2. Experimental

2.1. Growth of graphene

PMMA purchased from Aladdin was dissolved in anisole solvent to form 1 wt % solution and spin coating onto dielectric substrates with a thickness of ~15 nm. The PMMA film was subsequently heated to 65 °C in air to remove residual organic solvent. A 100 nm catalytic Nickel was deposited on the PMMA film by the electron beam evaporation. Then, 300 nm SiO_2 was deposited onto PMMA/Nickel via plasma enhanced chemical vapor deposition (PECVD; System 100, Oxford, UK). The layered structure of substrate/PMMA/Nickel/SiO_2 was annealed in N_2 using rapid thermal annealing (RTA) equipment (RTP600Z, Estarlabs, China) to convert PMMA into graphene. The samples were annealed at 800, 900, and 1000 °C for 90 s with an average heating rate of 10 °C/s. The conversion of graphene from PMMA was realized on various dielectric substrates such as sapphire, Si, quartz, and u-GaN. Besides, 2 inch sapphire was chosen as the wafer-scale substrate.

To remove Nickel/SiO_2 capping layer, the buffered oxide etch (BOE) was firstly applied to dissolve the SiO_2 layer, and then cleanly washed away by the deionized (DI) water. After that, the sample was immerged into a 0.5 mol/L $FeCl_3$ aqueous solution for 1 h to remove Nickel catalytic layer, and further 1 min ultrasonic cleaning in DI water was carried out to eliminate the surface pollution induced during $FeCl_3$ etching process. Thus, PMMA-converted graphene would be directly left on the surface of dielectric substrates.

2.2. Fabrication of u-GaN/graphene UV photodetector

After the growth of PMMA-converted graphene on u-GaN, a typical lithography technique was applied to prepare patterned photoresist masks on graphene. Afterwards, the interdigital electrodes composed of 30 nm Nickel/30 nm Gold were deposited on the top of u-GaN/graphene by the electron beam evaporation, which severed as contacted pads for the carrier collection. Then, the Nickel/Gold composite electrode was annealed in the RTA equipment at 550 °C for 5 min to form ohmic contact between graphene and metal electrodes. Here, interdigital electrodes had 25 pairs' fingers with line width and distance of both 5 μm, and the photosensitive area of UV photodetector was 0.2×0.5 mm^2. At the same time, an UV photodetector based on bare u-GaN has been fabricated for comparison.

2.3. Characterization and measurement

Raman spectrophotometer (LabRAM HR Evolution, HORIBA Scientific, UK) with a 532 nm laser was applied to measure the Raman spectra of PMMA and PMMA-converted materials. At the same time, 20×20 μm^2 Raman mapping of the intensity of D band (I_D), G band (I_G), 2D band (I_{2D}) as well as I_{2D}/I_G of graphene were measured by this Raman spectrophotometer, and the sampling interval was set as 1 μm. Atomic force microscope (AFM; MULTIMODE 8, Bruker, US) was used to analyze the surface morphology of various samples in tapping mode. The morphology characterization in large-area of these samples was also evaluated by optical microscope (OM; DS-Ri2, Nikon, Japan). The resistivity of graphene was obtained by a 4-probe resistivity measurement system (RTS-8, 4 Probes Tech, China). UV-vis spectrophotometer (UV-2550, SHIMADZU) was applied to measure the transmittance spectra of the as-grown graphene.

The UV photodetector based on the u-GaN integrated with the grown graphene was illuminated by a 266 nm laser (MPL-F-266-20mW, CNI Laser, China), the power intensity of laser was regulated to 10 mW and calibrated by a Wattmeter (TP100, CNI Laser, China). The dark current and photocurrent were measured by a 2400 Source Meter, KEITHLEY. The corresponding response time of photodetector was collected by a digital oscilloscope (DS6104, Rigol, China).

3. Results and discussion

The morphologies of PMMA, PMMA/Nickel, and PMMA/Nickel/SiO_2 on sapphire substrates were measured by atomic force microscope (AFM), as shown in Fig. S1a-c. All films exhibited the continuous surface, and the corresponding root-mean-square roughness (Rq) were 0.27, 1.10, and 3.64 nm, respectively. To verify the significance of Nickel catalytic metal with SiO_2 capping layer, we have compared the PMMA-converted materials with only Nickel catalytic layer and Nickel/SiO_2 capping layer, as shown in Fig. 1. Both samples of covered PMMA were annealed at 1000 °C for 60 s. Here, the only Nickel catalytic layer has deformed into separated particles with sizes varied from hundred nanometers to few micrometers because of its instability under high temperature treatment, as shown in Fig. 1a. PMMA-converted materials only existed under Nickel particles, and the difference in height between position A (without Nickel coverage) and B (with Nickel coverage)

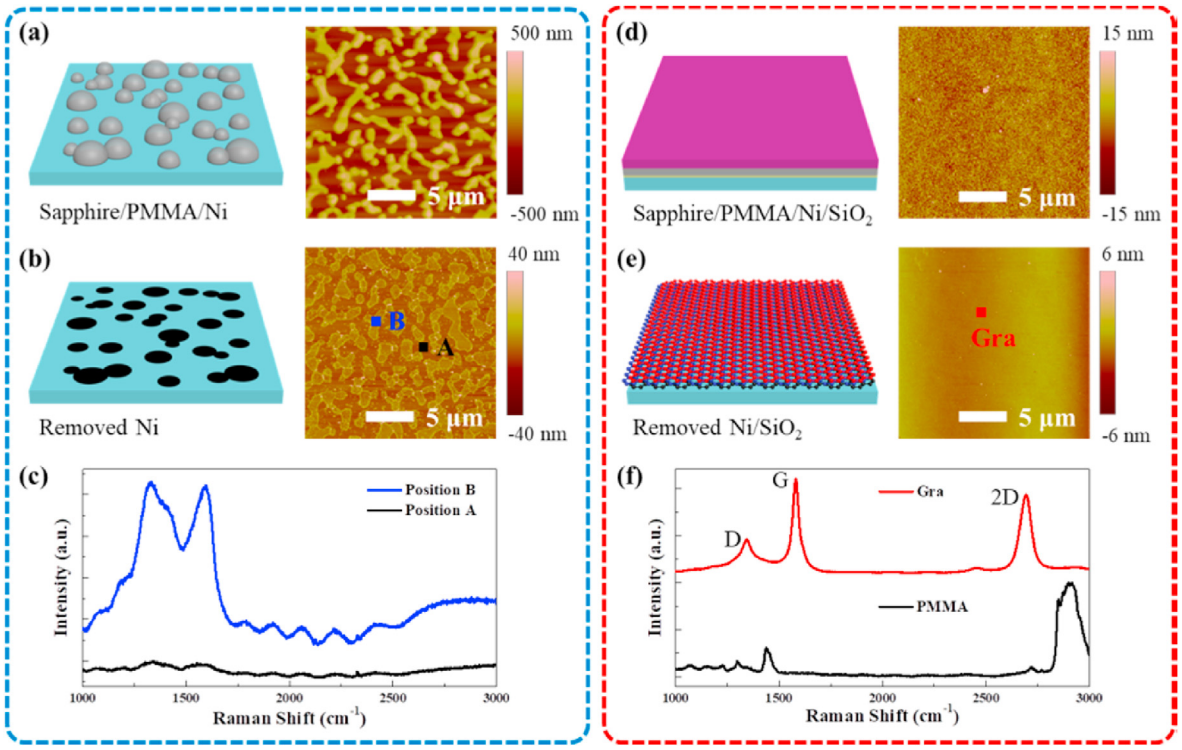

Fig. 1. (a) Schematic diagram and AFM images of the only Nickel catalytic layer on PMMA after high-temperature treatment and (b) after removing Nickel catalytic layer. (c) Raman spectra of PMMA-converted materials with the only Nickel catalytic layer. (d) Schematic diagram and AFM images of Nickel/SiO_2 capping layer on PMMA after high-temperature treatment and (e) after removing Nickel/SiO_2 capping layer. (f) Raman spectra of the grown few-layer graphene with Nickel/SiO_2 capping layer and bare PMMA. (A colour version of this figure can be viewed online.)

was around 5 nm, as shown in Fig. 1b. The corresponding morphology variation with the only Nickel catalytic layer was also confirmed by optical microscope (OM) in a larger view field, as shown in Fig. S2a and 2b. Raman spectra were applied to measure the structure properties of PMMA-converted materials, which would obtain the information of molecular vibration and rotation through Raman scattering effect. The Raman spectra of PMMA-converted materials with the only Nickel catalytic layer were shown in Fig. 1c. At position A, none visible signal band was observed at the wave number range of 1000–3000 cm^{-1}, which covered the typical bands of PMMA, amorphous carbon, and graphene [39]. This implied that carbon-related materials could not remain on the sapphire substrate without Nickel coverage, which might be evaporated and taken away from the surface of substrate by N_2 flow during RTA process. For position B, the PMMA-converted materials under Nickel particles only exhibited D and G bands located at 1332 and 1596 cm^{-1} with large full width at half maximum (FWHM) of 214.3 and 97.1 cm^{-1}, and the missing of 2D band implied that the PMMA-converted materials with the only Nickel catalytic layer was discontinuous amorphous carbon [40].

With the Nickel/SiO_2 capping layer, an integrated surface was observed by AFM, as shown in Fig. 1d. The additional SiO_2 layer have suppressed the deformation of the underneath Nickel layer, and thus providing uniformly catalytic condition for the PMMA conversion. The PMMA-converted material with the Nickel/SiO_2 capping layer also had a uniform and continuous morphology after removing Nickel/SiO_2 layers, and the Rq was only 0.73 nm, as shown in Fig. 1e. In addition, OM images in Fig. S2c and 2d also demonstrated these results. The corresponding Raman spectra appeared three typical peaks of graphene, which located at 1345 (D band), 1582 (G band), and 2688 cm^{-1} (2D band), as shown in Fig. 1f. The calculated intensity ratio of I_{2D}/I_G was lower than 1, indicating the few-layer nature of the grown graphene on sapphire substrates [41]. The continuous few-layer graphene film was scraped to create step edges, and the thickness of graphene was measured to be ~1.88 nm, as shown in Fig. S3. According to previous reports, this thickness measured by AFM in tapping mode corresponds to an approximate tri-layer graphene [42,43]. However, considering that the accuracy of graphene thickness measured by AFM in tapping mode was restricted by many factors, such as tip-surface interactions, image feedback settings and surface chemistry [44,45], the optical transparency of as-grown graphene was measured in Fig. S4. By the fact that the absorption of monolayer graphene is around 2.3%, the transmittance of 92.4% at 550 nm for as-grown graphene proved its tri-layer nature [46].

Although the grown graphene with the Nickel/SiO_2 capping layer exhibited excellent uniformity and continuity, the relatively high intensity of D band (related to defects) in Raman spectra indicated the inferior quality of as-grown graphene (Fig. 1f). Therefore, the RTA conditions of the graphene need to be controlled. Primarily, the growth temperature was adjusted by 800, 900, and 1000 °C with same RTA time of 60 s, and the corresponding Raman spectra were shown in Fig. 2a. The intensity ratio of I_D/I_G dramatically decreased from 1.3 to 0.35 as the growth temperature increased from 800 to 1000 °C, implying that high temperature acted as a key factor for better crystalline quality of the grown graphene. Moreover, the increased intensity of 2D band (I_{2D}/I_G: 0.19–0.83) as well as the reduced FWHM from 66.7 to 52.7 cm^{-1} implied that the fewer layer number of graphene was converted from PMMA at 1000 °C. In order to further improve the quality of graphene, PMMA with the Nickel/SiO_2 capping layer was annealed at 1000 °C for different growth time of 10, 30, and 90 s, and the corresponding Raman spectra of graphene was shown in Fig. 2b. The intensity ratio of I_D/I_G was calculated to be 0.63, 0.43, and 0.07

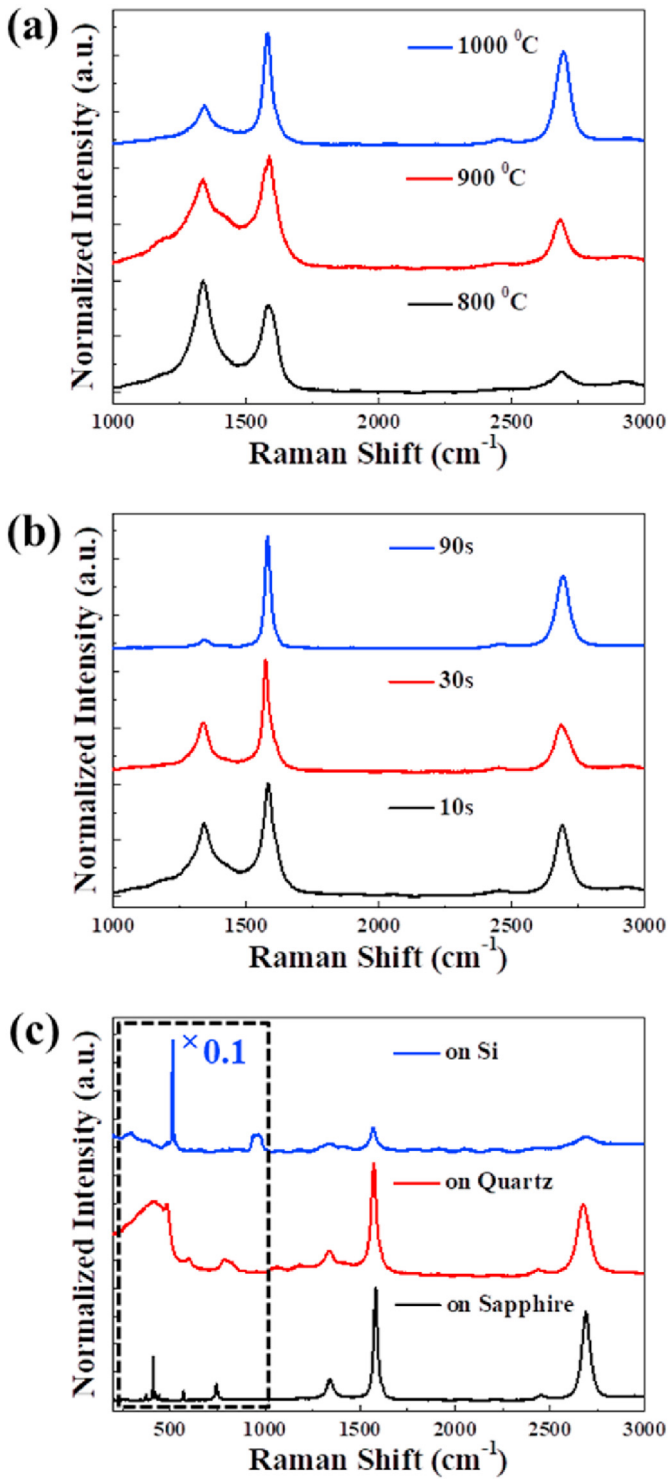

Fig. 2. (a) Raman spectra of the grown graphene converted from PMMA with Nickel/SiO_2 capping layer at different growth temperature, (b) growth time, and (c) on various dielectric substrates. (A colour version of this figure can be viewed online.)

for graphene grown by 10, 30, and 90 s, respectively. Among them, the grown graphene at the growth condition of 1000 °C/90 s possessed the lowest value of I_D/I_G, and it was even better than the CVD-grown graphene on catalytic Nickel substrates reported by previous works [47,48]. The Raman mapping of I_G and I_{2D} for PMMA-converted graphene at different annealing temperature and time were compared in Fig. S5 and S6, indicating that graphene with larger coverage and crystal domain size were achieved at higher annealing temperature and longer annealing time. Here, the higher temperature and longer annealing time might play key factors for the decomposition of polymer carbon source as well as the diffusion distance of the related carbon species which would affect the crystalline size and quality of grown graphene, and the corresponding growth mechanism would be discussed later in detail. The universality investigation of this growth of graphene on various dielectric substrates was carried out, and the corresponding Raman spectra were shown in Fig. 2c. Dielectric substrates with high melt point, including Si, quartz, and sapphire were applied, and the Raman spectra at the range of 200–1000 cm^{-1} (circled by black dashed line) exhibited typical bands of each dielectric substrate. All the grown graphene on these substrates exhibited typical G and 2D bands, while minor I_D was observed. Above results have demonstrated that high-quality few-layer graphene could be directly converted from PMMA with the Nickel/SiO_2 capping layer on various dielectric substrates.

The method of this grown graphene converted from PMMA with Nickel/SiO_2 capping layer was also evaluated on a 2 inch sapphire wafer, as shown in Fig. 3a. The corresponding photograph of few-layer graphene on sapphire (right) exhibited deeper color compared to the bare sapphire (left), which was mainly attributed to the light absorption of the grown graphene. Five points at the center and separated edges of wafer-scale graphene were selected for the Raman measurement, and the corresponding spectra were shown in Fig. 3b. All these positions of graphene exhibited typical D, G, and 2D bands with the few-layer nature, which indicated the large-area existence of graphene on the 2 inch sapphire wafer. Besides, the mean intensity ratio of I_D/I_G and I_{2D}/I_G were calculated to be 0.1 and 0.51, respectively. The corresponding minor standard deviations of 0.03 and 0.1 for I_D/I_G and I_{2D}/I_G have proved the uniformity of crystalline quality and layer number of the grown graphene. The Raman mapping of I_D, I_G, I_{2D} and I_{2D}/I_G were measured, as shown in Fig. 3c–f. The selected area of graphene possessed continuous intensity distribution, and the values of I_{2D}/I_G were homogeneous in the visible field. For comparison, we also measured the Raman mapping of CVD-grown graphene transferred onto sapphire substrates, as shown in Fig. S7a-d. The Raman mapping of the graphene converted from PMMA and CVD-grown graphene exhibited similar uniformity and continuity, which both had grain size of few micro-meters in bright spots. The electrical resistivity of the graphene was also compared with that graphene grown by CVD, as shown in Fig. S8. Five points were selected for accurate measurement, and the grown graphene and CVD-grown graphene transferred onto sapphire substrates exhibited the comparable electrical resistivity with mean values and standard deviations of 209.9 ± 14.4 and 160.4 ± 16.7 Ω • cm, respectively. Therefore, the graphene converted from PMMA with Nickel/SiO_2 capping layer was a reliable strategy for the growth of wafer-scale graphene on dielectric substrates. The uniformity, continuity as well as electrical properties of the grown graphene were good enough compared to that grown by conventional CVD method.

The typical Raman bands of graphene on top of Nickel after removing SiO_2 capping layer were also observed, as shown in Fig. 4a. The absent bands of underneath sapphire substrates confirmed that the typical Raman bands belonged to graphene above Nickel layer, rather than graphene at the interface of Nickel layer and sapphire substrates. According to the evidence of graphene converted from PMMA on both sides of Nickel layer, we have proposed the dynamics of the graphene growth, as shown in Fig. 4b. Initially, the PMMA source between Nickel catalytic layer and sapphire substrates was suffered from a carbonization process induced by the high temperature, in which PMMA molecular chains

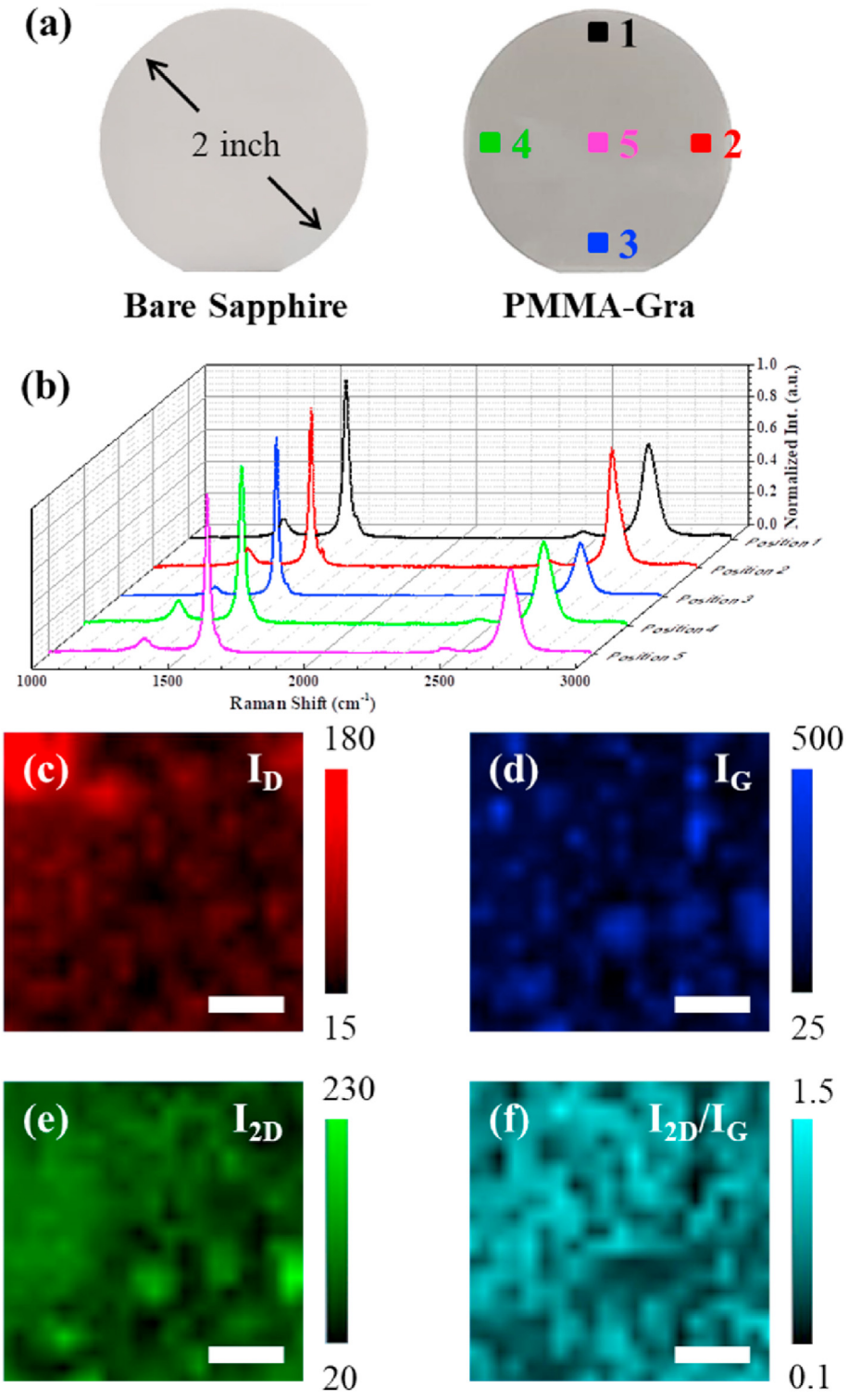

Fig. 3. (a) Photograph of bare 2 inch sapphire (left) and grown few-layer graphene on sapphire (right). (b) Raman spectra of five points derived from the 2 inch few-layer graphene on sapphire. (c) Raman mapping of the intensity of D band, (d) G band, (e) 2D band, and (f) intensity ratio of 2D band to G band. The scale bar is 5 μm. (A colour version of this figure can be viewed online.)

would break, and forming separated carbon atoms or related carbon fragments with the catalyst of Nickel, as shown in process ii of Fig. 4b. The carbon atoms possess a relatively high dissolvability in the bulk of Nickel films according to the previous work [49]. In this way, related carbon species would diffuse into the inside of Nickel layer with the persistent high temperature treatment, which should follow the direction from high carbon concentration to its absent sites, as shown in process iii of Fig. 4b. Here, the PMMA carbonization and carbon dissolution processes may not follow the exact sequential order. Otherwise, they probably happened at the same time. At the decreased temperature process, carbon atoms would be segregated and precipitated on both sides of Nickel

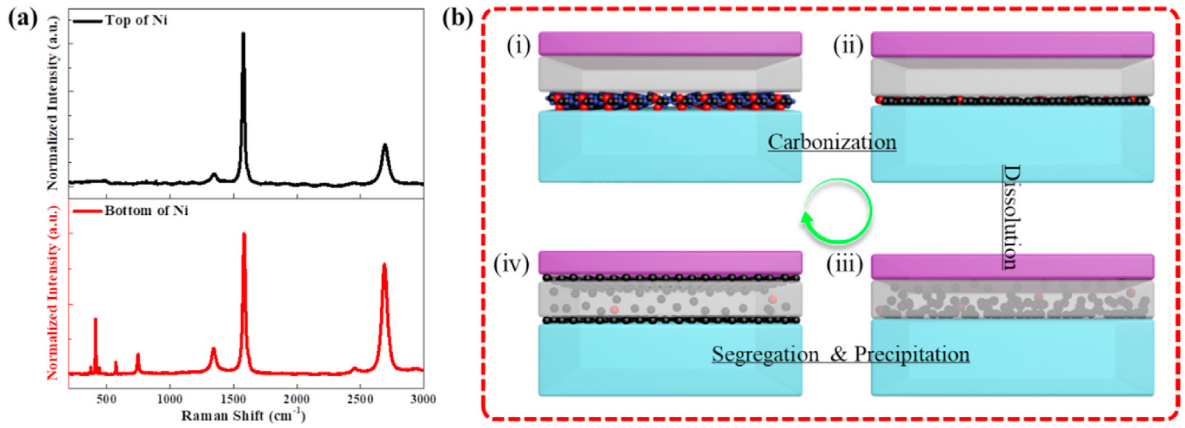

Fig. 4. (a) Raman spectra of the grown few-layer graphene on the top of Nickel catalytic layer and its bottom. (b) Schematic diagram of the dynamics of the growth process of PMMA-converted graphene with the Nickel/SiO_2 capping layer. (A colour version of this figure can be viewed online.)

catalytic layer, as shown in process iv of Fig. 4b. Previous works of saturated carbon in cooling Nickel foils also proposed the behaviors of carbon segregation and precipitation for monolayer graphite growth [50,51], which could be extended in this work. The precipitated carbon at the interfaces of sapphire/Nickel and Nickel/SiO_2 would be rearranged into graphene, and this was driven by the lattice effect of Nickel catalytic layer.

The excellent stability of Nickel/SiO_2 capping layer is crucial for sufficient PMMA catalytic decomposition as well as homogeneous carbon diffusion, which acts as important roles for high-quality graphene growth. For the only Nickel catalytic layer, it has been deformed into particles during the high temperature annealing, as shown in Fig. 1a. This process is usually named as the dewetting of metal films, which is driven by the reduction of the surface energy of metal films and the interface energy with the underneath substrates during the annealing treatment [52,53]. In present case, the annealing temperature of 1000 °C below the melting point of Nickel film (1453 °C) could also cause the dewetting by the activation energy induced diffusion, which is called solid-state dewetting [54]. With an additional SiO_2 capping layer, the dewetting of catalytic Nickel film was eliminated. Here, SiO_2 capping layer with good stability would not interact with the Nickel catalytic layer in both liquid and solid phases, and thus none degradation including oxidation or alloy formation could happen. At the same time, the viscous motion between the Nickel film and SiO_2 capping layer has ensured the integrity of the top SiO_2 in spite of the mechanical stress induced by Nickel melting and solidification [55]. For instance, the viscoelastic properties of SiO_2 was reported as 3.9×10^8 (Pa s) at the melting point of Nickel, and it dramatically dropped to 28.8 (Pa s) at the boiling point of Nickel (2913 °C) [56]. More importantly, the additional capping layer of SiO_2 has altered the surface free energy of the Nickel film, which increased the formation energy barrier of ruptures, ridges and particles related to the dewetting of metal films (see Part 2 in Supporting Information for the theoretical calculation) [57]. Therefore, the dewetting process of the Nickel/SiO_2 capping layer was suppressed compared to that only Nickel catalytic layer.

According to the dynamics of this growth process, the higher temperature and longer reaction time were key conditions for growth of high-quality graphene due to the requirement of the sufficient decomposition of PMMA molecule and enough dissolution distance for carbon species filtration. These results were consist with the experimental section of the graphene converted from PMMA, and the growth condition of 1000 °C/90 s possessed the best graphene crystalline quality. The higher temperature of 1000 °C has provided sufficient energy for PMMA decomposition, and the combination of longer annealing time of 90 s made purer carbon species through their diffusion in Nickel layer. This proposed growth dynamics provided a possible guidance for the controlled growth of graphene on dielectric substrates from the intrinsic physical mechanism.

Graphene with unbroken structures had a high carrier mobility, which possessed great potential as the charge transport channel of UV photodetectors with high response [58,59]. Here, we have fabricated u-GaN-based UV photodetectors with this grown graphene as the carrier transport channel, which have reduced the technique difficulty compared to CVD-grown graphene. The corresponding structure diagram and OM image of the as-fabricated UV photodetector were shown in Fig. 5a and b, respectively. A bare u-GaN on sapphire was simultaneously annealed in the RTA equipment during the growth of graphene, and interdigital Nickel/Gold composite electrodes were deposited on both samples as the charge collectors. The Raman spectra of bare u-GaN and *in situ* grown graphene on u-GaN were measured in Fig. 5c, and the typical Raman bands of u-GaN were observed and located at 567.4 and 734.7 cm^{-1}. At the same time, the typical G and 2D bands of graphene were also observed, which indicated the existence of few-layer graphene on u-GaN. The photocurrent (I_{ph}) of UV photodetectors without and with graphene was shown in Fig. 5d, which was calculated by $I_{ph} = I_{light} - I_{dark}$. Both UV photodetectors were measured with the bias voltage varied from 0 to 10 V, and the maximum values of I_{ph} for devices without and with graphene were 17.6 μA and 5.1 mA at 10 V, respectively. The response (R) was defined as $R = \frac{I_{ph}}{P \times A}$, P was the power density of incident UV laser, and A was the photosensitive area of photodetectors [60,61]. In this way, the response of UV photodetectors without and with the grown graphene was calculated to be 13.8 mA/W and 4 A/W, and the UV photodetector with the grown graphene exhibited two orders of magnitude enhancement in the response. This was attributed to the high carrier mobility and persistent photoconduction effect of graphene, and similar results were also reported by previous work [62,63]. The response time of these two types of photodetectors was also measured and shown in Fig. 5e. The rise time and fall time of photodetectors were defined as the time varied between the current of 10% and 90%. For device without graphene, its rise time and fall time were 7.2 and 6.8 ms, respectively. However, the UV photodetector with the graphene exhibited longer rise time and fall time of 18.2 and 7.2 ms. For the UV photodetector with PMMA-converted graphene as carrier transport channel, the photogenerated carriers in u-GaN absorber was drifted into graphene by

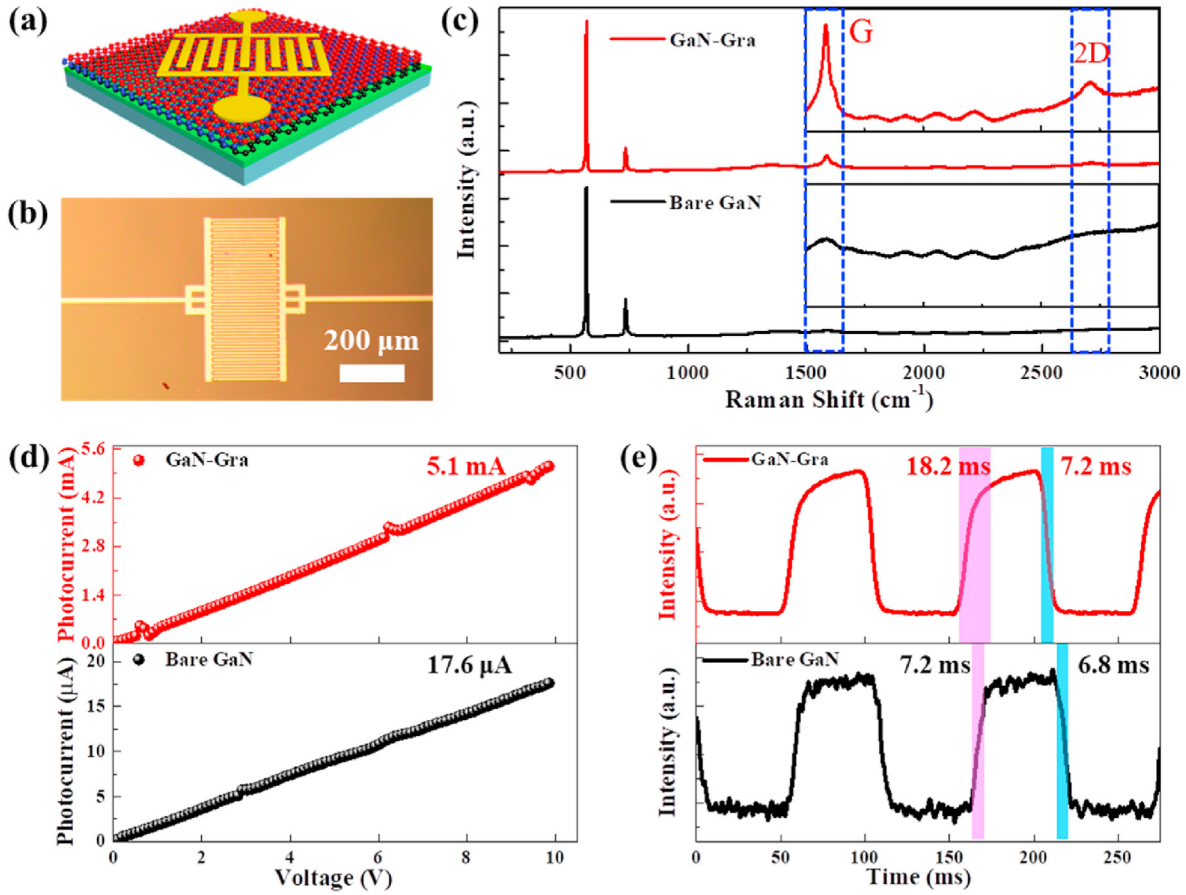

Fig. 5. (a) Schematic diagram of the device structure of u-GaN-based UV photodetector with the grown few-layer graphene as the carrier transport channel. (b) The corresponding OM image of the UV photodetector. (c) Raman spectra of bare u-GaN and grown few-layer graphene on u-GaN. (d) The photocurrent and (e) response time of UV photodetectors with and without the grown few-layer graphene. (A colour version of this figure can be viewed online.)

Table 1
Comparison of the response with previous works.

GaN Type	Graphene Type	Irradiation Source	Bias Voltage	Response	Ref.
Bulk GaN	w/o	325 nm Laser	5 V	633 mA/W	[8]
GaN Nanowire	Transferred (CVD)	357 nm LED	1 V	25 A/W	[58]
Bulk GaN	r-GO	340 nm Light	0 V	1.54 mA/W	[59]
Bulk GaN	Transferred (CVD)	325 nm Laser	10 V	361.3 mA/W	[62]
Bulk GaN	Transferred (CVD)	325 nm Laser	−10 V	5.83 A/W	[63]
Bulk GaN	Growth	266 nm Laser	10 V	4 A/W	**This Work**

the built-in field at the interface between u-GaN and graphene. Different from the limited carrier mobility of bare u-GaN, the photo-generated carriers could be circled in graphene for many times due to its high carrier mobility [63]. In this way, the UV photodetector with graphene exhibited larger response and longer response time.

In order to evaluate the effect of Nickel/SiO_2 capping layers, UV photodetectors were also fabricated on u-GaN with the surfaces of PMMA and PMMA/Nickel for comparison, as shown in Fig. S9. Here, without any capping layer, PMMA would be evaporated and taken away from u-GaN surface during the annealing process, as shown in Fig. 1c and Fig. S9a. For PMMA/Nickel surface, the deformed Nickel particle could make discontinuous amorphous carbon remaining on u-GaN surface, as shown in Fig. 1a–b and Fig. S9b. In this way, the UV photodetector with PMMA surface has exhibited the photocurrent and response of 26.3 μA and 20.6 mA/W, which was comparable to that of bare u-GaN-based device in Fig. 5d. The higher photocurrent and response of 623 μA and 489 mA/W were observed for the UV photodetector with PMMA/Nickel surface, which might be attributed to the existence of amorphous carbon on u-GaN surface. However, the response was still obviously inferior to the UV photodetector with PMMA/Nickel/SiO_2 surface by an order of magnitude. The UV photodetector based on PMMA/Nickel/SiO_2 surface with high response has further demonstrated the excellent crystalline quality of the few-layer graphene converted from PMMA by this strategy. In addition, the response of this UV photodetector was compared with previous works in Table 1, which exhibits similar or even better performance. Therefore, other types of device including high electron mobility transistors, LEDs and surface acoustic wave devices might be fabricated with this growth of graphene as the electrodes.

4. Conclusion

In conclusion, we reported the growth of high-quality few-layer graphene from the PMMA solid carbon source on dielectric substrates with the Nickel/SiO_2 capping layer. The growth conditions were optimized by growth temperature and time, and as-grown graphene exhibited better quality compared with the previously reported CVD-grown graphene. The successful growth of continuous and uniform graphene on the wafer-scale sapphire substrate proved the potential mass-production for this strategy. Besides, the dynamics of the growth process of this grown graphene were proposed, which was crucial for providing guidance of the growth of high-quality graphene. The graphene converted from PMMA was grown on u-GaN as a charge transport channel, and the as-fabricated UV photodetectors exhibited high response. This work has provided a simple and reliable method for graphene growth except conventional CVD, which exhibited potential for graphene-based electronic and optoelectronic devices.

Author contributions

The manuscript was written through contributions of all authors. All authors have given approval to the final version of the manuscript.

Declaration of competing interest

The authors declare that they have no known competing financial interests or personal relationships that could have appeared to influence the work reported in this paper.

Acknowledgements

This work was supported by the National Natural Science Foundation of China (61922078, 61827813, 61874118 61725403, 61704171, 52002368), National Key R&D Program of China (2017YFB0404103), Youth Innovation Promotion Association of the Chinese Academy of Sciences (Y201945), The Open Project of State Key Laboratory of Luminescence and Applications (E00522NZM100), Key-Area Research and Development Program of Guangdong Province (2020B010169001) and Suzhou Institute of Nano-Tech and Nano-Bionics (20YZ10).

Appendix A. Supplementary data

Supplementary data to this article can be found online at https://doi.org/10.1016/j.carbon.2020.12.055.

References

[1] K.S. Novoselov, A.K. Geim, S.V. Morozov, D. Jiang, Y. Zhang, S.V. Dubonos, et al., Electric field effect in atomically thin carbon films, Science 306 (5696) (2004) 666–669.
[2] L. Liao, Y.C. Lin, M.Q. Bao, R. Cheng, J.W. Bai, Y. Liu, et al., High-speed graphene transistors with a self-aligned nanowire gate, Nature 467 (7313) (2010) 305–308.
[3] J. Ning, Y. Wang, X. Feng, B.Y. Wang, J.G. Dong, D. Wang, et al., Flexible field-effect transistors with a high on/off current ratio based on large-area single-crystal graphene, Carbon 163 (2020) 417–424.
[4] A. Soltani, F. Kuschewski, M. Bonmann, A. Generalov, A. Vorobiev, F. Ludwig, et al., Direct nanoscopic observation of plasma waves in the channel of a graphene field-effect transistor, Light Sci. Appl. 9 (1) (2020) 97.
[5] G. Jo, M. Choe, C.Y. Cho, J.H. Kim, W. Park, S. Lee, et al., Large-scale patterned multi-layer graphene films as transparent conducting electrodes for GaN light-emitting diodes, Nanotechnology 21 (17) (2010), 175201.
[6] L.C. Wang, W. Liu, Y.Y. Zhang, Z.H. Zhang, S.T. Tan, X.Y. Yi, et al., Graphene-based transparent conductive Electrodes for GaN-based light emitting diodes: challenges and countermeasures, Nanomater. Energy 12 (2015) 419–436.
[7] J.S. Guo, J. Li, C.Y. Liu, Y.L. Yin, W.H. Wang, Z.H. Ni, et al., High-performance silicon-graphene hybrid plasmonic waveguide photodetectors beyond 1.55 μm, Light Sci. Appl. 9 (1) (2020) 29.
[8] S.K. Jain, S. Krishna, N. Aggarwal, R. Kumar, A. Gundimeda, S.C. Husale, et al., Effect of metal contacts on a GaN/Sapphire-Based MSM ultraviolet photodetector, J. Electron. Mater. 47 (10) (2018) 6086–6090.
[9] C.H. Liu, Y.C. Chang, T.B. Norris, Z.H. Zhong, Graphene photodetectors with ultra-broadband and high responsivity at room temperature, Nat. Nanotechnol. 9 (4) (2014) 273–278.
[10] Y. Chen, Y.Y. Yue, S.R. Wang, N. Zhang, J. Feng, H.B. Sun, Graphene as a transparent and conductive electrode for organic optoelectronic devices, Adv. Electron. Mater. 5 (10) (2019), 1900247.
[11] Y. Chen, X.Y. Fu, Y.Y. Yue, N. Zhang, J. Feng, H.B. Sun, Flexible and transparent supercapacitor based on ultrathin Au/graphene composite electrodes, Appl. Surf. Sci. 467 (2019) 104–111.
[12] X.Y. Zhang, S.H. Sun, X.J. Sun, Y.R. Zhao, L. Chen, Y. Yang, et al., Plasma-induced, nitrogen-doped graphene-based aerogels for high-performance supercapacitors, Light Sci. Appl. 5 (2016), e16130.
[13] X. Huang, Z.Y. Yin, S.X. Wu, X.Y. Qi, Q.Y. He, Q.C. Zhang, et al., Graphene-based materials: synthesis, characterization, properties, and applications, Small 7 (4) (2011) 1876–1902.
[14] H.L. Chang, Z.L. Chen, W.J. Li, J.C. Yan, R. Hou, S.Y. Yang, et al., Graphene-assisted quasi-van der Waals epitaxy of AlN film for ultraviolet light emitting diodes on nano-patterned sapphire substrate, Appl. Phys. Lett. 114 (9) (2019), 091107.
[15] Y.X. Feng, X.L. Yang, Z.H. Zhang, D. Kang, J. Zhang, K.H. Liu, et al., Epitaxy of single-crystalline GaN film on CMOS-compatible Si(100) substrate buffered by graphene, Adv. Funct. Mater. 29 (42) (2019), 1905056.
[16] Y. Chen, Y.P. Jia, Z.M. Shi, X.J. Sun, D.B. Li, Van der Waals Epitaxy: a new way for growth of III-nitrides, Sci. China-Tech. Sci. 63 (3) (2020) 528–530.
[17] Y. Arao, F. Mori, M. Kubouchi, Efficient solvent systems for improving production of few-layer graphene in liquid phase exfoliation, Carbon 118 (2017) 18–24.
[18] H.F. Yang, F. Withers, E. Gebremedhn, E. Lewis, L. Britnell, A. Felten, et al., Dielectric nanosheets made by liquid-phase exfoliation in water and their use in graphene-based electronics, 2D Mater. 1 (1) (2014), 011012.
[19] A. Dey, S. Krishnamurthy, J. Bowen, D. Nordlund, M. Meyyappan, R.P. Gandhiraman, Plasma jet printing and in situ reduction of highly acidic graphene oxide, ACS Nano 12 (6) (2018) 5473–5481.
[20] S.F. Pei, H.M. Cheng, The reduction of graphene oxide, Carbon 50 (9) (2012) 3210–3228.
[21] H. Huang, W. Chen, S. Chen, A.T.S. Wee, Bottom-up growth of epitaxial graphene on 6H-SiC(0001), ACS Nano 2 (12) (2008) 2513–2518.
[22] M. Sprinkle, M. Ruan, Y. Hu, J. Hankinson, M. Rubio-Roy, B. Zhang, et al., Scalable templated growth of graphene nanoribbons on SiC, Nat. Nanotechnol. 5 (10) (2010) 727–731.
[23] I.V. Vlassiouk, Y. Stehle, P.R. Pudasaini, R.R. Unocic, P.D. Rack, A.P. Baddorf, et al., Evolutionary selection growth of two-dimensional materials on polycrystalline substrates, Nat. Mater. 14 (4) (2018) 318–322.
[24] S. Naghdi, K. Yop Rhee, S.J. Park, A catalytic, catalyst-free, and roll-to-roll production of graphene via chemical vapor deposition: low temperature growth, Carbon 127 (2018) 1–12.
[25] S. Pezzini, V. Miseikis, G. Piccinini, S. Forti, S. Pace, R. Engelke, et al., 30°-Twisted bilayer graphene quasicrystals from chemical vapor deposition, Nano Lett. 20 (5) (2020) 3313–3319.
[26] X.S. Li, L. Colombo, R.S. Ruoff, Synthesis of graphene films on copper foils by chemical vapor deposition, Adv. Mater. 28 (29) (2016) 6247–6254.
[27] X.S. Li, Y.W. Zhu, W.W. Cai, M. Borysiak, B.Y. Han, D. Chen, et al., Transfer of large-area graphene films for high-performance transparent conductive electrodes, Nano Lett. 9 (12) (2009) 4359–4363.
[28] G. Deokar, J. Avila, I. Razado-Colambo, J.L. Codron, C. Boyaval, E. Galopin, et al., Towards high quality CVD graphene growth and transfer, Carbon 89 (2015) 82–92.
[29] J.Y. Sun, Y.B. Chen, M. Kr Priydarshi, T. Gao, X.J. Song, Y.F. Zhang, et al., Graphene glass from direct CVD routes: production and applications, Adv. Mater 28 (46) (2016) 10333–10339.
[30] X.D. Chen, Z.L. Chen, W.S. Jiang, C.H. Zhang, J.Y. Sun, H.H. Wang, et al., Fast growth and broad applications of 25-inch uniform graphene glass, Adv. Mater. 29 (1) (2017), 1603428.
[31] S. Suzuki, Y. Takei, K. Furukawa, H. Hibino, Graphene growth from a spin-coated polymer without a reactive gas, APEX 4 (6) (2011), 065102.
[32] Z.Z. Sun, Z. Yan, J. Yao, E. Beitler, Y. Zhu, J.M. Tour, Growth of graphene from solid carbon sources, Nature 468 (7323) (2010) 549–552.
[33] Q.Q. Zhuo, Q. Wang, Y.P. Zhang, D. Zhang, Q.L. Li, C.H. Gao, et al., Transfer-free synthesis of doped and patterned graphene films, ACS Nano 9 (1) (2015) 594–601.
[34] M. Xu, J. Feng, Y.S. Liu, Y. Jin, H.Y. Wang, H.B. Sun, Effective and tunable light trapping in bulk heterojunction organic solar cells by employing Au-Ag alloy nanoparticles, Appl. Phys. Lett. 105 (15) (2014), 153303.
[35] Y.F. Li, J. Feng, F.X. Dong, R. Ding, Z.Y. Zhang, X.L. Zhang, et al., Surface plasmon-enhanced amplified spontaneous emission from organic single crystals by integrating graphene/copper nanoparticle hybrid nanostructures, Nanoscale 9 (48) (2017) 19353–19359.
[36] S.K. Lim, K.S. Ban, Y.H. Kim, C.K. Kim, C.S. Yoon, S. Jin, Monolayered Ni–Co alloy nanoparticles template fabricated using a Ni nanoparticle array, Appl. Phys. Lett. 88 (16) (2006), 163102.

[37] A. Kathalingam, H.M.S. Ajmal, S. Ramesh, H.S. Kim, S.D. Kim, S.H. Choi, et al., Poly(methyl methacrylate)-derived graphene films on different substrates using rapid thermal process: a way to control the film properties through the substrate and polymer layer thickness, J. Mater. Res. Technol. 8 (5) (2019) 3752–3763.
[38] S.J. Byun, H. Lim, G.Y. Shin, T.H. Han, S.H. Oh, J.H. Ahn, et al., Graphenes converted from polymers, J. Phys. Chem. Lett. 2 (5) (2011) 493–497.
[39] A. Sadezky, H. Muckenhuber, H. Grothe, R. Niessner, U. Pöschl, Raman micro spectroscopy of soot and related carbonaceous materials: spectral analysis and structural information, Carbon 43 (8) (2005) 1731–1742.
[40] A.C. Ferrari, J. Robertson, Interpretation of Raman spectra of disordered and amorphous carbon, Phys. Rev. B 61 (20) (2000) 14095–14107.
[41] Y.F. Hao, Y.Y. Wang, L. Wang, Z.H. Ni, Z.Q. Wang, R. Wang, et al., Probing layer number and stacking order of few-layer graphene by Raman spectroscopy, Small 6 (2) (2010) 195–200.
[42] D. Graf, F. Molitor, K. Ensslin, C. Stampfer, A. Jungen, C. Hierold, et al., Spatially resolved Raman spectroscopy of single- and few-layer graphene, Nano Lett. 7 (2) (2007) 238–242.
[43] J. Li, H.X. Ji, X. Zhang, X.Y. Wang, Z. Jin, D. Wang, et al., Controllable atmospheric pressure growth of mono-layer, bi-layer and tri-layer graphene, Chem. Commun. 50 (75) (2014) 11012–11015.
[44] P. Nemes-Incze, Z. Osváth, K. Kamarás, L.P. Biró, Anomalies in thickness measurements of graphene and few layer graphite crystals by tapping mode atomic force microscopy, Carbon 46 (11) (2008) 1435–1442.
[45] C.J. Shearer, A.D. Slattery, A.J. Stapleton, J.G. Shapter, C.T. Gibson, Accurate thickness measurement of graphene, Nanotechnology 27 (12) (2016) 125704.
[46] W. Wu, Q.K. Yu, P. Peng, Z.H. Liu, J.M. Bao, S.S. Pei, Control of thickness uniformity and grain size in graphene films for transparent conductive electrodes, Nanotechnology 23 (3) (2012), 035603.
[47] L.X. Cheng, K. Yun, A. Lucero, J. Huang, X. Meng, G.D. Lian, et al., Low temperature synthesis of graphite on Ni films using inductively coupled plasma enhanced CVD, J. Mater. Chem. C 3 (20) (2015) 5192–5198.
[48] A. Umair, H. Raza, Controlled synthesis of bilayer graphene on nickel, Nanoscale Res. Lett. 7 (2012) 437.
[49] X.S. Li, W.W. Cai, L. Colombo, R.S. Ruoff, Evolution of graphene growth on Ni and Cu by carbon isotope labeling, Nano Lett. 9 (12) (2009) 4268–4272.
[50] J.C. Shelton, H.R. Patil, J.M. Blakely, Equilibrium segregation of carbon to a nickel (111) surface: a surface phase transition, Surf. Sci. 43 (2) (1974) 493–520.
[51] M. Eizenberg, J.M. Blakely, Carbon interaction with nickel surfaces: monolayer formation and structural stability, J. Chem. Phys. 71 (8) (1979) 3467–3477.
[52] D. Wang, P. Schaaf, Solid-state dewetting for fabrication of metallic nanoparticles and influences of nanostructured substrates and dealloying, Phys. Status Solidi 210 (8) (2013) 1544–1551.
[53] A. Herz, F. Theska, D. Rossberg, T. Kups, D. Wang, P. Schaaf, Solid-state dewetting of Au–Ni bi-layer films mediated through individual layer thickness and stacking sequence, Appl. Surf. Sci. 444 (2018) 505–510.
[54] A.L. Giermann, C.V. Thompson, Solid-state dewetting for ordered arrays of crystallographically oriented metal particles, Appl. Phys. Lett. 86 (12) (2005), 121903.
[55] J.E. Kline, J.P. Leonard, Suppression of dewetting in pulsed laser melting of thin metallic films on SiO_2, Mater. Res. Soc. Symp. Proc. 854 (2004) U11.6.
[56] J.E. Kline, J.P. Leonard, Suppression of dewetting phenomena during excimer laser melting of thin metal films on SiO_2, Thin Solid Films 488 (2005) 306–313.
[57] D.J. Srolovitz, M.G. Goldiner, The thermodynamics and kinetics of film agglomeration, JOM 47 (3) (1995) 31–36.
[58] A.V. Babichev, H. Zhang, P. Lavenus, F.H. Julien, A. Yu Egorov, Y.T. Lin, et al., GaN nanowire ultraviolet photodetector with a graphene transparent contact, Appl. Phys. Lett. 103 (20) (2013) 201103.
[59] N. Prakash, M. Singh, G. Kumar, A. Barvat, K. Anand, P. Pal, et al., Ultrasensitive self-powered large area planar GaN UV-photodetector using reduced graphene oxide electrodes, Appl. Phys. Lett. 109 (24) (2016) 242102.
[60] G. Nazir, M.F. Khan, I. Akhtar, K. Akbar, P. Gautam, H. Noh, et al., Enhanced photoresponse of ZnO quantum dot-decorated MoS_2 thin films, RSC Adv. 7 (27) (2017) 16890–16900.
[61] G. Nazir, M.A. Rehman, M.F. Khan, G. Dastgeer, S. Aftab, A.M. Afzal, et al., Comparison of electrical and photoelectrical properties of ReS_2 field-effect transistors on different dielectric substrates, ACS Appl. Mater. Interfaces 10 (38) (2018) 32501–32509.
[62] H.J. Tian, Q.L. Liu, A.Q. Hu, X.Y. He, Z.H. Hu, X. Guo, Hybrid graphene/GaN ultraviolet phototransistors with high responsivity and speed, Optic Express 26 (5) (2018) 5408–5415.
[63] H.J. Tian, Q.L. Liu, C.X. Zhou, X.J. Zhan, X.Y. He, A.Q. Hu, et al., Hybrid graphene/unintentionally doped GaN ultraviolet photodetector with high responsivity and speed, Appl. Phys. Lett. 113 (12) (2018), 121109.